Spin Crossover in the 2,2′-Bipyrimidine- (bpym-) Bridged Iron(II) Complexes $[Fe(L)(NCX)_2]_2(bpym)$ (L = 2, 2′-Bithiazoline (bt) and bpym; X = S, Se). X-ray Absorption Spectroscopy, Magnetic Susceptibility, Calorimetric, and Mössbauer Spectroscopy Studies

José Antonio Real,*[,1a] Isabel Castro,[1a] Azzedine Bousseksou,[1b] Michel Verdaguer,[1c] Ramón Burriel,[1d] Miguel Castro,[1d] Jorge Linares,[1e] and François Varret[1e]

Departament de Química Inorgánica, Universitat de València, 46 100 Burjassot (València), Spain, Laboratoire de Chimie de Coordination du CNRS, UP 8241, 205 route de Narbonne, 31077 Toulouse, France, Laboratoire de Chimie des Métaux de Transition URA CNRS 419, Université Pierre et Marie Curie, 4 place Jussieu, 75252 Paris Cédex 05, France, Instituto de Ciencia de Materiales de Aragón, CSIC-Universidad de Zaragoza, 50009 Zaragoza, Spain, and Laboratoire de Magnétisme et d'Optique, CNRS, URA 1531, Université de Versailles, 45 Av. des États Unis, 78035 Versailles, France

Received May 9, 1996[⊗]

This contribution is concerned with the synthesis and characterization of two new iron(II) spin-crossover dinuclear compounds of the formula $[Fe(bpym)(NCSe)_2]_2$ (bpym) (**2**) and $[Fe(bt)(NCSe)_2]_2(bpym)$ (**4**), where bpym = 2,2′-bipyrimidine and bt = 2,2′-bithiazoline. Evidence for a $S = 2$ (high spin, HS) ↔ $S = 0$ (low spin, LS) spin-crossover behavior is provided by variable-temperature magnetic susceptibility measurements and ^{57}Fe Mössbauer spectrometric data. Compound **2** shows only one step which involves 50% of the iron(II) ions. The transition is very abrupt and takes place at $T_c \approx 120$ K when cooling and shows a hysteresis loop of 2.5 K. A two-step spin transition takes place for **4**. The first one occurs at 223 K and the second one at 265 K. Differential scanning calorimetry exhibits two peaks in the case of **4**, a sharp one at 225 K and a broad one with a maximum at 262 K. ΔH and ΔS variations, per mol of dinuclear units, have been evaluated accurately for the first peak only, 5.7 ± 0.5 kJ mol^{-1} and 25.5 ± 1 J mol^{-1} K^{-1}, respectively. A rough estimate of the global variations gave 16 kJ mol^{-1} and 65 J mol^{-1}K^{-1}, respectively. Thermodynamic parameters, per mol of dinuclear units, for **2** are ΔH = 3.0 ± 0.1 kJ mol^{-1} and $\Delta S = 25 \pm 1$ J mol^{-1} K^{-1}. X-ray absorption spectroscopy has been carried out for **2** and **4** as well as for the parent compounds $[Fe(bpym)(NCS)_2]_2(bpym)$ (**1**) and $[Fe(bt)(NCS)_2]_2(bpym)$ (**3**). The X-ray absorption near edge structures spectra of the two spin isomers are interpreted and the extended X-ray absorption fine structures spectra are analyzed quantitatively at the first coordination shell. The average Fe−N bond distance is close to 0.2 Å larger for the HS state than that of the LS state. The spin transitions in these dimeric compounds are interpreted in terms of LS−LS ↔ LS−HS and LS−HS ↔ HS−HS intramolecular processes.

Introduction

Electronic spin-crossover phenomenon is a type of molecular magnetism[2,3] that occurs in some six-coordinate first-row transition metal complexes as the result of an electronic instability that is driven by external constraints (temperature, pressure, or electromagnetic radiation)[4−6] that induce structural changes at both the molecular and lattice levels.[7] Six-coordinate iron(II) ($3d^6$) spin-crossover compounds are among the most investigated systems; they reversibly change from diamagnetic ($S = 0$) to paramagnetic ($S = 2$) spin states. In the solid state, a cooperative first-order spin transition (ST) takes place at a well-defined critical temperature for a few of these compounds, some of which show thermal hysteresis.

We have attempted to clarify the nature of the cooperative mechanism in spin-crossover systems by correlating the structural changes with magnetic susceptibility, Mössbauer spectroscopy, and calorimetry data.[8,9] The aim is to define the main factors that control the abruptness, hysteresis, and critical temperature in order to design new materials that might be used in molecular devices. Up to now, the major source of information on ST systems comes from mononuclear iron(II) compounds where, because of the spin conversion, molecular distortions spread through the whole crystal by means of intermolecular interactions. The cooperativity in these systems would be enhanced by controlling both intra and intermolecular interactions. Cooperativity can be achieved by using suitable bridging ligands. As a first step along this line, we synthesized a series of dimeric iron(II) spin-crossover compounds of the formula $[Fe(L)(NCS)_2]_2(bpym)$, where bpym (2,2′-bipyrimidine) is the bis-bidentate bridging ligand and L is bpym (**1**),[10] bromazepan (bzp),[10] and bt (2,2′-bithiazoline, **3**).[11] Compound **1** is a high-spin (HS) complex showing a weak intramolecular antiferromagnetic interaction, whereas the bzp derivative and compound **3** show singlet−quintet spin conversion. The bzp

[⊗] Abstract published in *Advance ACS Abstracts,* December 15, 1996.

(1) (a) Universitat de València. (b) Laboratoire de Chimie de Coordination. (c) Université Pierre et Marie Curie. (d) Universidad de Zaragoza. (e) Université de Versailles.
(2) *Theory and Applications of Molecular Paramagnetism;* Boudreaux, E. A., Mulay, L. N., Eds.; Wiley: New York, 1976.
(3) Kahn, O. *Molecular Magnetism;* VCH Publishers: New York, 1993.
(4) Gütlich, P. *Struct. Bonding* (*Berlin*) **1981**, *44*, 83. Gütlich, P.; Hauser, A.; Spiering, H. *Angew. Chem., Int. Ed. Engl*. **1994**, *33*, 2024.
(5) König, E. *Struct. Bonding (Berlin)* **1991**, *76*, 51.
(6) Gütlich, P.; Hauser, A. *Coord. Chem. Rev*. **1990**, 97, 1.
(7) König, E. *Prog. Inorg. Chem*. **1987**, *35*, 527.
(8) Gallois, B.; Real, J. A.; Hauw, C.; Zarembowitch, J. *Inorg. Chem.* **1990**, *20*, 1152.
(9) Real, J. A.; Gallois, B.; Granier, T.; Suez-Panamá, F.; Zarembowitch, J. *Inorg. Chem.* **1992**, 31, 4972.
(10) Real, J. A.; Zarembowitch, J.; Kahn, O.; Solans, X. *Inorg. Chem*. **1987**, *26*, 2939.
(11) Real, J. A.; Bolvin, H.; Bousseksou, A.; Dworkin, A.; Kahn, O.; Varret, F.; Zarembowitch, J. *J. Am. Chem. Soc.* **1992**, *114*, 4650.

S0020-1669(96)00509-5 CCC: $14.00

derivative undergoes an incomplete spin conversion, and only half of the iron(II) ions are involved in the spin change. In contrast to **1** and the bzp derivative, **3** shows the remarkable feature of the occurrence of an almost complete double-step spin transition. The two-step character was analyzed in the framework of the Slichter and Drickamer model starting from the hypothesis that conversion takes place in the following two steps: LS (low spin)−LS ↔ LS−HS and LS−HS ↔ HS−HS. The stabilization of the LS−HS state could result from the synergistic effect between intramolecular and intermolecular interactions. An equivalent Ising−like model has been also used.[12]

The present work was undertaken with two main objectives in mind. One is to extend the number of dinuclear iron(II) spin-crossover compounds in order to confirm the observed phenomenology on bt and bzp derivatives. The other consists of following the structural changes that are associated with the spin conversion as closely as possible in order to confirm the above mentioned hypothesis, particularly the existence of the LS−HS species. So, in this paper we report on the synthesis and characterization of two new spin-crossover compounds, namely $[Fe(bpym)(NCSe)_2]_2(bpym)$ (**2**) and $[Fe(bt)(NCSe)_2]_2$-(bpym) (**4**), which are different from **1** and **3** in that the NCS^- groups have been replaced by $NCSe^-$ ones. The unavailability of single crystals moved us to use X-ray absorption spectroscopy for their structural characterization. Therefore, an important part of this work deals with the analysis and discussion of the structural features of compounds **1**−**4**, paying special attention to their changes upon the spin conversion. This structural investigation is completed by magnetic measurements and calorimetric and Mössbauer experiments.

Experimental Section

Synthesis and Characterization. The synthesis of **1** and **3** was carried out as previously reported.[10,11] Compounds **2** and **4** were synthesized by following a slightly modified procedure. Compound **2** was obtained as follows: a methanolic solution (15 mL) of $[Fe(H_2O)_6](ClO_4)_2$ (153.12 mg, 0.422 mmol) was added to a solution of KNCSe (121.6 mg, 0.844 mmol) in the same solvent (15 mL). The mixture was stirred for 15 min and was filtered to remove the $KClO_4$ precipitated. A methanolic solution (10 mL) of bpym (100 mg, 0.633 mmol) was added dropwise to the resulting methanolic solution which contains a 1:2 iron(II)/$NCSe^-$ ion ratio. Precipitation of **2** as a black microcrystalline powder, along with partial precipitation of a red solid (1:3 iron to bpym compound), followed immediately. The red solid evolved to **2** after stirring and warming for 15 min. Compound **4** was obtained in a similar way, but in the first step, a solution of bt (108.87 mg, 0.633 mmol) in methanol/dichloromethane (80:20, 30 mL) was added dropwise. The final solution was stirred for 10 min, and the solution was kept at 60 °C until a black microcrystalline product was formed. The precipitates were filtered and dried with an argon stream. Anal. Calcd for $C_{28}H_{18}N_{16}Se_4Fe_2$ (**2**): C, 33.4; H, 1.8; N, 22.3. Found: C, 32.7; H, 2.1; N, 21.6. Anal. Calcd for $C_{24}H_{22}N_{12}S_4Se_4Fe_2$ (**4**): C, 27.8; H, 2.1; N, 16.2. Found: C, 27.6; H, 1.8; N, 16.1.

X-ray Absorption Data Recording and Processing. The XANES (X-ray absorption near edge structures) and EXAFS (extended X-ray absorption fine Structures) data were collected at LURE (Laboratoire d'Utilisation du Rayonnement Electromagnetique, Paris-Sud University) on a storage ring with an energy of 1.85 GeV and a mean intensity of 300−200 mA. The measurements were carried out at the iron K-edge in the transmission mode on the EXAFS III spectrometer equipped with a two-crystal monochromator (Si 311, 0.5 mm entrance slit for both XANES and EXAFS). The monochromator was slightly out of tune to ensure harmonics rejection. Reduced-pressure, air-filled ionization chambers were used to measure the flux intensity before and after the sample. The spectra were recorded at room temperature and 77 K in a nitrogen cryostat that was designed for X-ray absorption spectroscopy.

The XANES spectra were recorded step by step, every 0.25 eV with a 1 s accumulation time per point. The spectrum of a 5 μm thick iron foil was recorded just after or before an unknown XANES spectrum to check the energy calibration, thus ensuring an energy accuracy of 0.25 eV. The EXAFS spectra were recorded in the same way over 1000 eV, with 2 eV steps and 1 s accumulation time per point. The experiments were calibrated by using the 8991.1 eV peak at the top edge of a metallic foil of copper and verifying that the first inflection point in all of the spectra of the iron foils was 7111.2 eV. Samples were well-pounded microcrystalline powders of a homogeneous thickness and calculated weight that were compressed between two X-ray transparent windows. The thickness was computed to avoid saturation effects. The absorbance jump at the edge was typically 1. Each spectrum is the sum of several independent recordings added after individual inspection (two for XANES and four for EXAFS).

XANES spectra were processed by substracting a linear background computed by least-squares fitting from the pre-edge experimental points and normalized by using the atomic absorption background as the unit absorbance. The energy of the pre-edge transition was determined by fitting the experimental curves with polynomial functions and taking the first and the second derivatives. EXAFS data analysis was carried out by following a well-known procedure described elsewhere.[13] It includes the following: (i) data reduction from $\mu(E)$ (linear X-ray absorption coefficient) to $k\chi(k)$, where $\chi(k)$ is the EXAFS modulation above the photoelectron energy threshold E_0 (taken at the absorption maximum) and k the photoelectron wave vector $k = [(2m_e/h^2)(h\nu - E_0)]^{1/2}$; (ii) Fourier transform of $k^3\chi(k)$ to obtain the radial distribution $F(R) = \mathrm{FT}[k^3\chi(k)]$; (iii) Fourier filtering of the first FT peak (Kaiser window, $\tau = 3.5$); and (iv) least-squares fitting of the filtered spectra to the standard EXAFS formula

$$k\chi(k) = -S_0^2 \sum_j \frac{N_j}{R_j^2} |f_j(\pi,k)| e^{-2\sigma_j^2 k^2} e^{-2R_j/\lambda_j(k)} \sin[2kR_j + 2\partial(k) + \Psi_{ij}(k)]$$

where S_0^2 is the inelastic reduction factor ($S_0^2 = 1$ in our fits), N_j represents the number of atoms at the distance R_j from the iron absorber, σ_j is the Debye−Waller coefficient, a damping coefficient due to thermal and structural distribution of distances, λ_j is the mean-free path of the photoelectron, $f_j(\pi,k)$ is the backscattering amplitude of neighbor j, $\partial_i(k)$ is the central atom phase shift, and $\Psi_{ij}(k)$ is the phase shift function for absorber−neighbor pairs. The spherical-waves theoretical amplitudes and phase shifts calculated by McKale[14] were used. Therefore, it was necessary to fit the photoelectron energy threshold E_o by adding an extra fitting parameter ΔE_o. The reliability of the fits was determined by the least-squares fitting parameter, ρ, defined as

$$\rho(\%) = \sum [k\chi_{\mathrm{exp}}(k) - k\chi_{\mathrm{th}}(k)]^2 / \sum [k\chi_{\mathrm{exp}}(k)]^2$$

The XANES[15a] and EXAFS[15b] analysis used a chain of programs written by Michalowicz on a Macintosh microcomputer. The EXAFS chain

(12) (a) Bousseksou, A.; Nasser, J.; Linares, J.; Boukheddaden, K.; Varret, F. *J. Phys. I* **1992**, *2*, 1381. (b) Bousseksou, A.; Varret, F.; Nasser, J. *J. Phys., I* **1993**, *3*, 1463.

(13) (a) Brown, G. S.; Doniach, S. In *Synchrotron radiation spectroscopy research*; Winick, J., Doniach, S., Ed.; Plenum Press: New York, 1981; pp 353−383. (b) Teo, B. K. *EXAFS Spectroscopy*; Plenum Press: New York, 1981. (c) Stern, E. A.; Head, S. M. In *Handbook on Synchrotron Radiation*; North Holland Publishing Company: Amsterdam, 1983; pp 955−1014. (d) Teo, B. K. *EXAFS: basic principles and data analysis*; Inorganic chemistry concepts; Springer−Verlag: Berlin, 1986, Vol. 9. (e) Michalowicz, A.; Verdaguer, M.; Mathey, Y.; Clement, R. In *Current Topics in Chemistry*; Mandelkow, H., Ed.; Springer: Berlin, 1988; Vol. 145, p 107.

(14) McKale, A. G.; Veal, B. W.; Paulikas, A. P. *J. Am. Chem. Soc.* **1988**, *110*, 3763.

(15) (a) Noinville, V.; Michalowicz, A. GALAAD. In *Logiciels pour la Chimie;* Société Française de Chimie: Paris, 1991; pp 116−117. (b) Michalowicz, M. EXAFS pour le MAC. *Ibid.* pp 102−103.

is associated with the MINUIT function minimization program.[16a] The modeling of the outer shells is not possible in the frame of the single-scattering model, and the multiple scattering/spherical-waves EXAFS *ab initio* modeling FEFF program was used.[16b] These calculations were performed on a RISC system/6000 running AIX 3.2.5 of the Physical Chemistry Department of the University of Valencia. The amplitudes and phase shifts extracted from FEFF calculation were then used to fit the outer shells. Multiple scattering (MS) EXAFS contributions were included using methodology described elsewhere.[16c] As expected for single-backscattering fits, the differences between both sets of results for the first shell are always within the error bars.

Magnetic Susceptibility Measurements. The variable-temperature magnetic susceptibility measurements were carried out on polycrystalline samples over the temperature range 4.2−300 K with a fully automated AZTEC DSM8 pendulum-type susceptometer equipped with a TBT continuous-flow cryostat and a Brüker BE15 electromagnet operating at 1.8 T. The apparatus was calibrated with mercury tetrakis(thiocyanato)cobaltate(II). Experimental susceptibilities were corrected for diamagnetism of the constituent atoms by the use of Pascal's constants.

Mössbauer Spectra. The variable-temperature Mössbauer measurements were obtained on a constant-acceleration conventional spectrometer with a 25 mCi source of ^{57}Co (Rh matrix). Isomer shift values (IS) are given with respect to the metallic iron at room temperature. The absorber was a sample of about 100 mg of microcrystalline powder of **2** or **4** enclosed in a 2−cm-diameter cylindrical plastic sample holder, the size of which had been determined to optimize the absorption. Variable-temperature spectra were obtained in the 305−4.2 K range by using a MD306 Oxford cryostat; the thermal scanning was monitored by an Oxford ITC4 servocontrol device (±0.1 K accuracy). A least-squares computer program[17] was used to fit the Mössbauer parameters and to determine their standard deviations of statistical origin (given in parentheses).

Differential Scanning Calorimetry (DSC). Calorimetric measurements have been performed on **2** and **4** using a differential scanning calorimeter Perkin-Elmer DSC-7. Low temperatures were obtained with an aluminium block attached to the sample holder, refrigerated with a flow of liquid nitrogen, and controlled at a temperature of 77 K. The sample holder was kept in a drybox with a flow of dry nitrogen to avoid water condensation. The measurements were carried out using between 10 and 30 mg of powdered samples that were sealed in aluminium pans with a mechanical crimp. Temperature and enthalpy calibrations were made with standard samples of cyclohexane by using its melting (279.69 K, 2678 J mol^{-1}) and crystal-to-crystal transitions (186.10 K, 6740 J mol^{-1}). An empty pan and a synthetic sapphire sample were also measured for each sample thermogram to ensure the accuracy of the heat capacity results. An overall accuracy of ±0.2 K in temperature and ±2% in the heat capacity is estimated in the whole temperature range. Enthalpy and entropy variations are given per mole of dinuclear units.

Results and Discussion

X-ray Absorption Studies (XANES and EXAFS). Structure Investigation. In the present family of compounds of the formula $[Fe(L)(NCX)_2]_2(bpym)$, only the X-ray single-crystal structure of **1** is known.[10] The molecular unit is sketched in Figure 1 and consists of centrosymmetric bpym-bridged iron(II) dinuclear entities. The intramolecular metal−metal separation is 5.522(6) Å. Two NCS^- ligands in the *cis* position and a peripheral bpym ligand acting as a bidentate ligand complete the octahedron around each metal ion. The Fe−N(CS) bond distances (2.051(7) and 2.078(6) Å for Fe−N(2) and Fe−N(1),

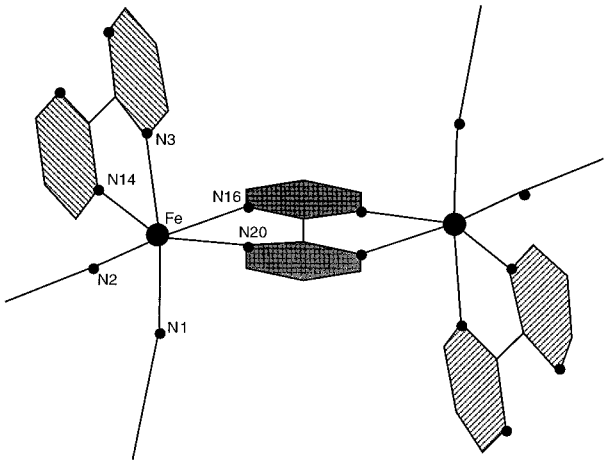

Figure 1. Perspective drawing of $[Fe(bpym)(NCS)_2]_2(bpym)$ molecular unit.

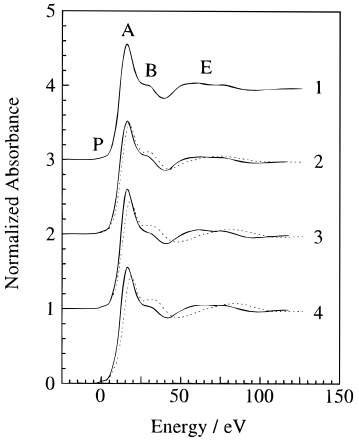

Figure 2. XANES spectra of complexes **1**−**4** at 300 K (solid line) and of complexes **2**−**4** at 77 K (dotted line): P, pre-edge; A, top of the edge; B, shoulder; E, first EXAFS oscillation.

respectively) are significantly smaller than those of Fe−N(bpym) [2.200(6), 2.211(6), and 2.223(6) Å for Fe−N(3), Fe−N(14), and Fe−N(20), respectively, and an axial one Fe−N(16) = 2.316(20) Å, the largest Fe−N bond distance in the octahedron]. As we could not grow crystals of compounds **2**−**4** that were suitable for X-ray diffraction studies, we turned toward EXAFS spectroscopy at the iron K-edge. This technique provides the possibility to evaluate the changes at the iron local environment upon transition, using powder samples. In order to check the validity of the EXAFS data analysis method, we also studied the X-ray diffraction structurally characterized compound **1**.

Figure 2 displays the normalized XANES spectra at 300 K for compounds **1**−**4** and at 77 K for **2**−**4**. Values of the energies and estimates of the intensity of the main features of the edge are displayed in Table 1. At first glance, some apparent features may be pointed out by comparing these spectra: (i) curves 2, 3, and 4 show the effect of the temperature on the edge of the absorption and the first EXAFS oscillation for **2**−**4**, both shift to higher energies as a consequence of the decreasing Fe−N distances that are associated with the spin conversion (see Table 1); (ii) a similar change is observed in the spectra when comparing compounds **1** and **2** at 300 K and **3** and **4** at 300 or 77 K that is associated with the pseudohalide change. The experimental $k\chi(k)$ spectra at 300 K for compounds **1**−**4** and at 77 K for **2**−**4** are given in the Supporting Information (Figure S1). The corresponding radial distributions and the experimental and calculated $k\chi(k)$ values for the filter of the first shell at both temperatures are presented in Figure 3. The number and postulated nature of neighbors, absorber−neighbor

(16) (a) James, F.; Roos, M. MINUIT program, a system for function minimization and analysis of the parameters errors and correlations. *Comput. Phys. Commun.* **1975**, *10*, 345. (b) Rehr, J. *Jpn. J. Appl. Phys.* **1993**, *32*, 8. (c) Michalowicz, A.; Moscovici, J.; Ducourant, B.; Cracco, D.; Kahn, O. *Chem. Mater.* **1995**, *7*, 1833.

(17) Varret, F. *Proceedings of the International Conference on Mössbauer Effect Applications*, Jaipur, India, 1981; Indian National Science Academy: New Delhi, 1982.

Table 1. Energy and Relative Intensity of the XANES Spectra

complex	energy/eV (relative intensity)			
	pre-edge (P)	top of the edge (A)	shoulder (B)	first EXAFS oscillation (E)
		300 K		
1	7113.2 (vw)[a]	7127.8(1.56)[b]	7139.6(1.01)	7172.4(1.03)−7186.7(1.01)
2	7113.4 (vw)	7128.0(1.52)	7139.7(1.05)	7174.0(1.04)−7186.8(1.03)
3	7113.7 (vw)	7128.1(1.60)	7140.5(1.03)	7174.2(1.06)−7187.2(1.05)
4	7113.8 (vw)	7128.3(1.56)	7140.7(1.04)	7174.9(1.05)−7187.6(1.05)
		77 K		
2	7113.8 (vw)	7129.4(1.49)	7140.2(1.10)	7175.8(1.03)−7187.8(1.05)
3	7114.0 (vw)	7130.0(1.44)	7140.0(1.12)	7175.6(1.00)−7193.1(1.07)
4	7114.2 (vw)	7130.6(1.44)	7140.7(1.12)	7177.0(0.99)−7196.4(1.07)

[a] vw: Very weak. [b] Absorbance, relative to the atomic absorption taken as unit.

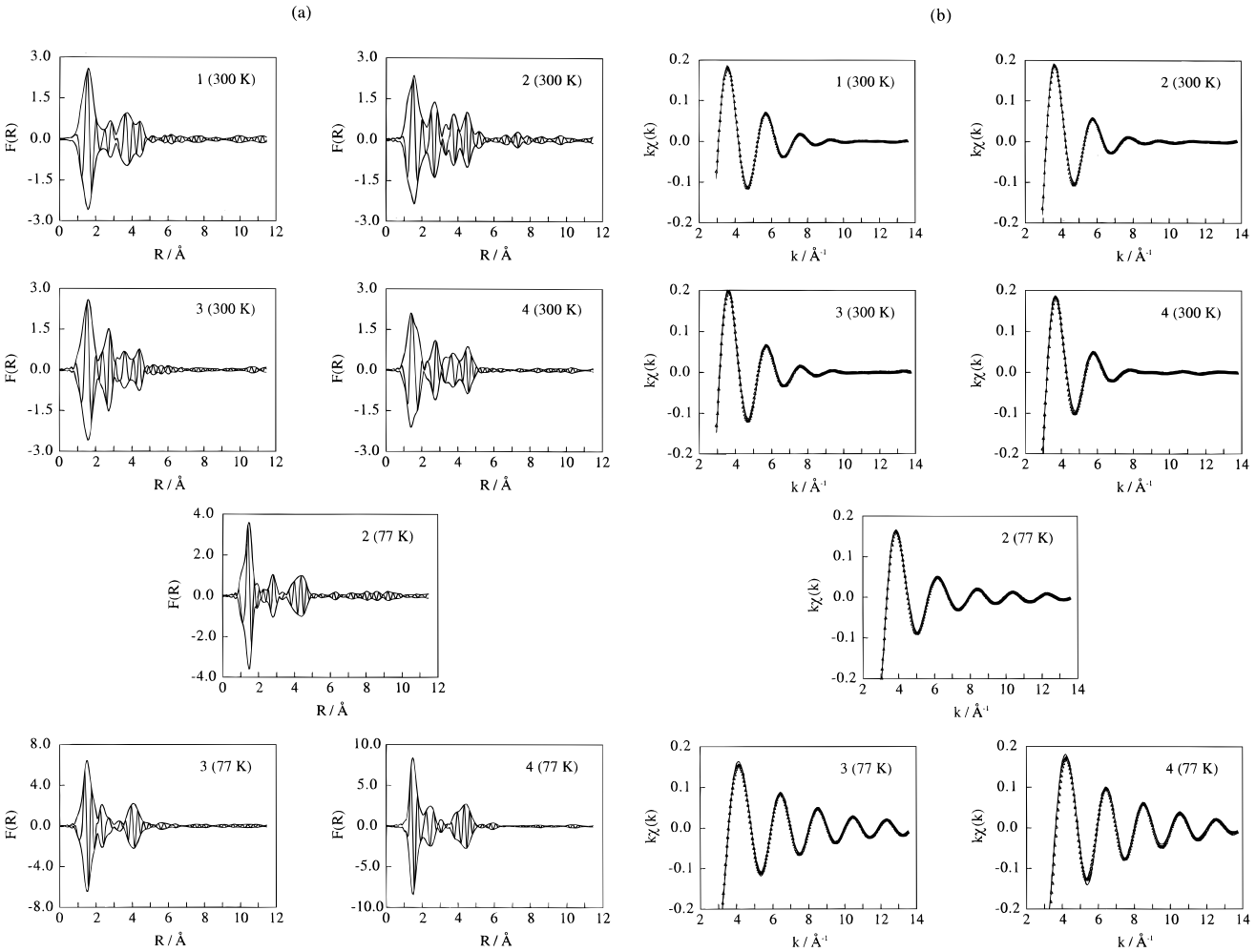

Figure 3. (a) Fourier transforms of the EXAFS spectra of complexes **1**−**4** at 300 K and of complexes **2**−**4** at 77 K including the modulus and imaginary parts. (b) Comparaison of the experimental and calculated $k\chi(k)/k$ values for the first filtered shell of complexes **1**−**4** at 300 K and of complexes **2**−**4** at 77 K (△ experimental, ○ calculated) (Figure 3 b).

distances, Debye−Waller factors, and other parameters resulting from quantitative analyses of the EXAFS data for the first shell are gathered in Table 2. In order to avoid apparent good fits without physical meaning, the number of fitted parameters was constrained to the minimum (in particular, we chose the same values of Γ and $E°$ for the three subshells and kept the scale factor equal to 1) and the experimental data were fitted with the various distributions of atom absorber−neighbors distances (2N + 4N, 4N + 2N, 2N + 3N + 1N, and 2N + 2N + 2N), see Table 2, based on the molecular structures of **1** and Fe(bt)$_2$(NCS)$_2$,[18] to have starting values of the Fe−N distances. The agreement factors were only slightly different from each other in some of these attempts. The most likely atomic distribution, summarized in Table 2, is based not only on the results of the fits but also on the Mössbauer and X-ray diffraction data and chemical arguments. On the |F(R)| spectra, each atomic shell surrounding the iron is represented by a peak: the first one corresponds to nitrogen atoms of both the bridging and peripheral ligands, which belong to the coordination sphere of the metal ion, the second and third peaks include essentially carbon and nitrogen atoms of the bpym, bt, and pseudohalide groups, and the significant signal present at a distance between 4 and 5 Å is due to the heavy S/Se atoms of the NCS/NCSe ligands as the major contribution. We only quantitatively analyzed the first shell of neighbors. We did not attempt to analyze the remaining ones because our interest is the study of the structural changes that are associated with the spin conversion. Moreover, multiple scattering is very important further

Table 2. Parameters Resulting from the Analysis of the First Shell EXAFS Data

	complex						
	300 K				77 K		
parameters[a]	**1**	**2**	**3**	**4**	**2**	**3**	**4**
	First Subshell						
no. and postulated nature of neighbors	2N	2N	2N	2N	2N	2N	2N
R_1 (Å)	2.06(1)	2.03(1)	2.06(1)	2.01(1)	1.99(1)	1.97(1)	1.94(1)
σ_1 (Å)	0.08	0.09	0.08	0.08	0.07	0.04	0.01
	Second Subshell						
no. and postulated nature of neighbors	3N	2N	2N	2N	2N	2N	2N
R_2 (Å)	2.19(2)	2.16(1)	2.15(1)	2.15(1)	2.10(1)	1.97(1)	1.94(1)
σ_2 (Å)	0.08	0.08	0.08	0.06	0.07	0.04	0.01
	3rd Subshell						
no. and postulated nature of neighbors	1N	2N	2N	2N	2N	2N	2N
R_3 (Å)	2.30(2)	2.28(2)	2.25(2)	2.27(2)	2.19(2)	2.10(1)	2.08(1)
σ_3 (Å)	0.09	0.11	0.10	0.11	0.07	0.04	0.01
E° (eV)	7127	7128	7128	7128	7130	7130	7131
Γ	1.1	1.1	1.1	1.1	1.2	1.4	1.5
ρ (%)	0.5	0.5	0.4	0.6	0.4	0.4	1.0

[a] The fitted parameters are as follows: the Fe−N distances, R_i; the Debye−Waller factors, σ_i; the ionization energy, E°; the constant Γ used to define the free mean path of the electron ($\lambda(k) = (1/\Gamma)[(\eta/k)^4 + k]$) with $\eta = 3.1$. The agreement factor is $\rho = \sum_{k(\min)}^{k(\max)}(\chi_{exp} - \chi_{th})^2/\sum_{k(\min)}^{k(\max)}\chi_{exp}^2$ with $k(\min) = 3$ Å^{-1} and $k(\max) = 14$ Å^{-1}. Standard deviations in distances are in parentheses.

Table 3. Relevant EXAFS (Compounds **1**−**4**) and X-ray Diffraction (Compounds **1**, **5**−**9**) Structural Data of Iron(II) Complexes

	room temperature			low temperature			ΔR upon HS-to-LS conversion		
		d [Fe−N(L)]			d [Fe−N(L)]			ΔR [Fe−N(L)]	
	d [Fe−NCX]	L (peripheral)	L (bridge)	d [Fe−NCX]	L (peripheral)	L (bridge)	ΔR [Fe−NCX]	L (peripheral)	L (bridge)
$[Fe(bpym)_2(NCS)_2](bpym)$ (**1**)[10]	2.06 (2.065)[a]	2.19 (2.206)[a]	2.25	(2.270)[a]					
$[Fe(bpym)_2(NCS_e)_2](bpym)$ (**2**)	2.03	2.16	2.28	1.99	2.10	2.19	0.04(0.08)[b]	0.06(0.12)[b]	0.09(0.18)[b]
$[Fe(bt)_2(NCS)_2](bpym)$ (**3**)	2.06	2.15	2.25	1.97	1.97	2.10	0.09	0.18	0.15
$[Fe(bt)_2(NCS_e)_2](bpym)$ (**4**)	2.01	2.15	2.27	1.94	1.94	2.08	0.07	0.21	0.19
$[Fe(phen)_2(NCS)_2]$ (**5**)[8]	2.057	2.206		1.958	2.009		0.099	0.197	
$[Fe(bipy)_2(NCS)_2]$ (**6**)[18]	2.053	2.173		1.945	1.966		0.108	0.207	
$[Fe(btz)_2(NCS)_2]$ (**7**)[9]	2.064	2.170		1.948	1.973		0.116	0.197	
$[Fe(tap)_2(NCS)_2]CH_3CN$ (**8**)[20]	2.057	2.214		1.937	1.983		0.120	0.231	
$[Fe(bt)_2(NCS)_2]$ (**9**)[17]	2.070	2.202							

[a] X-ray diffraction data. [b] The values in parentheses correspond to the ΔR expected for 100% HS-to-LS conversion.

from the first shell, and the modeling of the outer shells is not possible in the frame of the simple scattering model.

The relevant structural EXAFS data and the assignment of each subshell along with single-crystal X-ray data of some significant monomeric spin-crossover systems that are related to the title compounds are grouped in Table 3. The first subshell, with an average bond distance ranging from 2.01(1) to 2.06(1) Å at room temperature, has been ascribed to the Fe−N(CX) metal to ligand bond distance. In particular, when X = *S* (**1** and **3**), the bond distance compares well with that of compounds $[Fe(phen)_2(NCS)_2]$,[8] $[Fe(btz)_2(NCS)_2]$,[9] $[Fe_2(bpym)_3(NCS)_4]$,[10] $[Fe(bt)_2(NCS)_2]$,[18] $[Fe(bipy)_2(NCS)_2]$,[19] and $[Fe(tap)_2(NCS)_2]$[20] (phen = 1,10-phenanthroline, btz = 2,2′-bi-4,5-dihydrothiazine, bipy = 2,2′-bipyridine, tap = 1,4,5,8-tetraazaphenanthrene). As far as the Fe−N(CSe) value is concerned, compounds **2** and **4** show Fe−N distances slightly shorter than the Fe−N(CS) ones for **1** and **3**. Due to the lack of structural information about the Fe−N(CSe) bond length in other iron(II) compounds, we cannot compare the experimental data. However, our results are coherent with the experimental fact that the $NCSe^-$ group induces a stronger ligand field than that for NCS^-. The room temperature, average Fe−N bond distance that is assigned to the bidentate ligands is *ca.* 2.20(1) Å. The splitting of these values into their components Fe−N (peripheral) and Fe−N (bridge) gives satisfactory values since the metal−bridge distances are reasonably larger (*ca.* 2.25(1)−2.27(1) Å) than the metal−peripheral ligand ones (*ca.* 2.15(1) Å). Compounds **2**, **3**, and **4** undergo spin change at low temperature. The changes in the molecular structure that are associated with the spin conversion involve shortening of the Fe−N distances and changes in N−Fe−N and Fe−N−(CX) angles.[7] Consequently, the $[FeN_6]$ chromophore is less distorted after the spin conversion. All of these facts are reflected in Table 3 and are consistent with those obtained from the diffraction methods for related spin-crossover compounds.[8−10,18−20]

A semiquantitative analysis of the last Fourier transform peak to check the presence of Fe−Fe pairs reveals that this signal is due to two sulphur atoms at *ca.* 4.7 Å for both compounds **1** and **3** and to two selenium atoms at *ca.* 4.9 Å for **2** and **4**. The difference between the Fe−S and Fe−Se distances is thus on the order of 0.2 Å. This variation is the same as that observed in the compounds $[Mn(bpym)(NCX)_2]_2(bpym)$ (X = S, Se).[21]

(18) Ozarowski, A.; McGarvey, B. R.; Sarkar, A. B.; Drake, J. E. *Inorg. Chem.* **1988**, *27*, 628.
(19) Konno, M.; Mikami-Kido, M. *Bull. Chem. Soc. Jpn.* **1991**, *64*, 339.
(20) Real, J. A.; Muñoz, M. C.; Andrés, E.; Granier, T.; Gallois, B. *Inorg. Chem.* **1994**, *33*, 3587.

After the HS-to-LS conversion, the Fe−S/Se distances are shorter, as expected, 4.4 Å for compound **3** (Fe−S) and 4.8 Å for **2** and **4** (Fe−Se).

The main features of the XANES spectra and a simple interpretation of them are given hereafter. The most characteristic absorptions observed near the edge are essentially originated by the transitions of the excited photoelectrons from the 1s core orbital to the vacant levels of the proper symmetry (bound states). Four parts can be arbitrarily distinguished in the edge spectrum: the pre-edge structures, the rising edge, the top of the edge, and finally the post-edge structures. We take the iron K-edge energy, 7112 eV, as the energy origin, and we assign this, for each structure, as the lowest and highest energy in complexes **1**−**4** for the HS (LS) species, taking into account that for complex **1**, only the HS form exists.

The weak pre-edge transition at 1.2−1.8 eV for the HS species (1.8−2.2 eV LS) can be safely assigned to the symmetry-forbidden electronic dipolar transitions 1s → "3d MO′". 3d MO′ refers to the excited molecular levels that are centered on the 3d molecular orbitals of the iron(II). The prime sign means that in the excited state, the MOs are relaxed in the core hole. The low intensity is typical for forbidden transitions in metal complexes in a quasi-centrosymmetric geometry (idealized O_h symmetry). Whatever the spin state, only four vacant 3d levels are available in the d^6 electronic configuration of Fe(II). In the HS state, the transitions are to t_{2g} and e_g MO′s. They appear wider and at lower energy than those in the LS state $(t_{2g})^6$, when they occur to the fully vacant e_g MO′s only. In the HS spectra, the underlying multiplet structure is unresolved, given the weakness of the transition and the experimental resolution (*ca.* 0.25 eV or more). Therefore, the pre-edge energy differences that are observable in Table 1 are to be used with caution since they have been determined on weak, poorly defined features.

The strong absorption at 15.8−16.3 (17.4−18.6) eV corresponds to the symmetry-allowed electronic dipolar transitions 1s → 4p MO′. In both the HS and LS states, the distortion of the coordination sphere is not sufficiently pronounced to resolve the three transitions 1s → $4p_x$ MO′, 1s → $4p_y$ MO′, and 1s → $4p_z$ MO′. However, the distribution of the distances is large enough to widen the transition. The value of the intensity at the top of the edge is less than that observed in the parent Fe(II) compounds,[22] which is likely due to a larger distortion and less participation of the 4p (Fe) orbital in the MO′ level. The main changes upon the HS-to-LS conversion are safely explained: (i) the 2 eV shift to higher energy (from *ca.* 16 eV for the HS species to *ca.* 18 eV for the LS ones) is due to the shortening of the metal−ligand distances (destabilization of the energy of the 4p MOs and enhanced antibonding character); (ii) the clear decrease in intensity is a consequence of a decreased participation of the 4p metal orbitals through the enhanced metal−ligand overlap; (iii) the smaller width likely indicates a lower distortion of the coordination core in the LS form (see Table 2).

The medium intensity feature at 28−29 eV, above the ionization energy, is assigned to a multiple-scattering process. Its intensity is enhanced in the LS form (likely due to closer neighbors and lower Debye−Waller factors).

The spectra are completed by the first EXAFS oscillation, which is displaced from *ca.* 68 (HS) to 80 eV (LS). The strong shift toward higher energies is due to the shortening of the metal−ligand distances, upon HS-to-LS conversion. The oscillation exhibits several components in both the HS and LS form spectra, which correspond to a distribution of the iron−neighbor distances in each of the compounds. The fact that these structures are more important in the HS forms than in the LS ones points out a lower distortion of the coordination core in the second ones. The long distances disappear in the LS forms.

Finally, other structures are present in the rising edge, in both HS and LS spectra. Two-electrons transitions (shake-downs), transitions to d−π* levels, have been postulated to interpret them. Since this assignment is not important to continue further in the quantitative analysis of the spin conversion, we prefer to remain prudent.

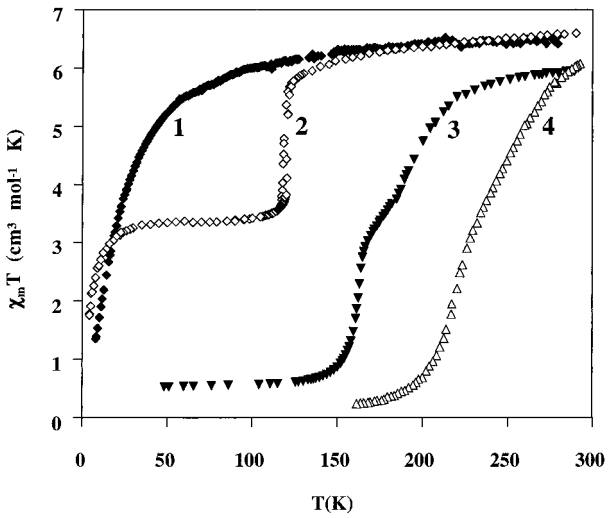

Figure 4. Thermal variation of the $\chi_m T$ product obtained from magnetic susceptibility measurements of **1**−**4**.

Magnetic Susceptibility Data. The thermal dependence of the product $\chi_M T$ (χ_M being molar susceptibility) for compounds **1**−**4** is displayed in Figure 4.

The $\chi_M T$ value for **1** at room temperature is 6.53 cm^3 mol^{-1} K. This value decreases upon cooling and vanishes as T approaches to zero. This behavior is characteristic of an intramolecular antiferromagnetic interaction between two high-spin iron(II) ions with a low-lying spin singlet as the ground state. The experimental data were quantitatively interpreted by means of the spin Hamiltonian $\boldsymbol{H} = -J\boldsymbol{S}_A\boldsymbol{S}_B + g\beta(\boldsymbol{S}_A + \boldsymbol{S}_B)H$ obtaining $J = -4.1$ cm^{-1} and $g = 2.13$ as the best parameters.[10] No spin transition occurs in this compound.

The magnetic behavior of **2** is similar to that of **1** in the 290−175 K temperature range. The value of $\chi_M T$ is *ca.* 6.6 cm^3 mol^{-1} K at room temperature, and it diminishes more rapidly upon cooling, reaching a value around 5.8 cm^3 mol^{-1} K at 125 K. The $\chi_M T$ product decreases suddenly down to 3.5 cm^3 mol^{-1} K in the 125−115 K temperature region, providing evidence for a $S = 2 \leftrightarrow S = 0$ spin crossover. The warming mode reveals the occurrence of a 2.5 K wide thermal hysteresis (≈5 h to run the full hysteresis loop), where $T_c(\uparrow)$ and $T_c(\downarrow)$ are *ca.* 122.5 and 120 K, respectively. Seventy percent the spin conversion occurs within an interval of 5 K. All of these features are indicative of a strong cooperative first-order spin transition. At low temperature, the residual high-spin fraction was estimated to be around 50%, the same value was obtained from the Mössbauer measurements (see below). A further $\chi_M T$ decrease takes place in the 30−4.2 K temperature range. This behavior is most likely due to the local anisotropy of the remaining 50% high-spin iron(II) ions, since the Mössbauer spectra of **2** confirms the existence of 50% high-spin Fe(II) ions at 4.2 K.

The magnetic properties of **3** have already been studied previously in detail.[11] The $\chi_M T$ value at room temperature is

(21) De Munno, G.; Julve, M. Personal communication.
(22) Roux, C.; Zarembowitch, J.; Itié, J. P.; Polian, A.; Verdaguer, M. *Inorg. Chem.* **1996**, *35*, 574.

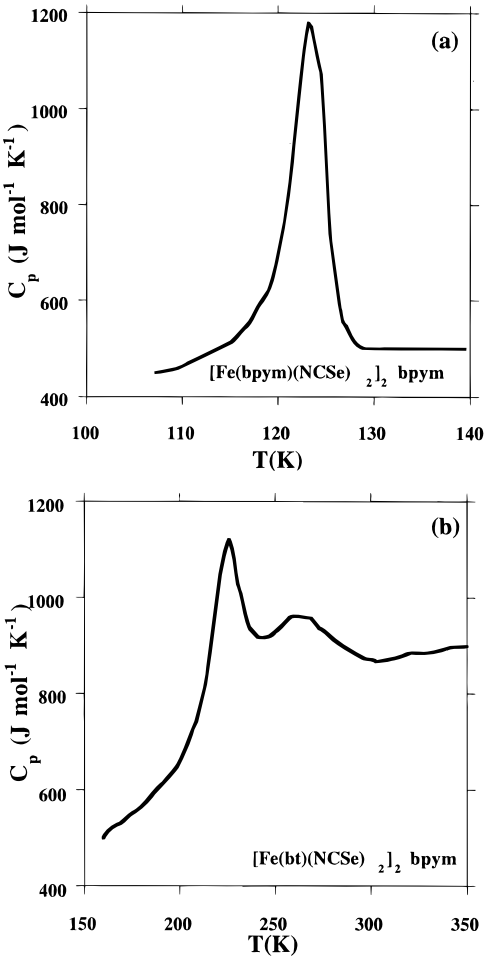

Figure 5. DSC curves for **2** (a) and **4** (b), obtained in the heating mode.

5.98 cm^3 mol^{-1} K, with a small amount of low-spin (*ca.* 9%) iron(II) ions remaining at this temperature. At 100 K, $\chi_M T$ is 0.53 cm^3 mol^{-1} K, a value which is characteristic of low-spin iron(II) with residual amounts of the high-spin form, *ca.* 8%. The spin conversion does not noticeably present thermal hysteresis but shows the remarkable singularity taking place in the two steps mentioned above; step 1 and step 2 are centered around the temperatures 163 and 197 K, respectively. The former is rather abrupt, 80% of the spin change occurring within *ca.* 15 K; the latter is smoother. The intermediate plateau between the two spin conversions (*ca.* 169−181 K) at a value of $\chi_M T$ *ca.* 3.35 cm^3 mol^{-1} K corresponds to a high-spin iron(II) fraction of *ca.* 50%. Finally, compound **4** has a magnetic behavior analogous to that of **3** but the spin conversion starts at a higher temperature. At 290 K, the value of $\chi_M T$ is close to 5.9 cm^3 mol^{-1} K which involves 12% low-spin iron(II) ions (low-spin content at room temperature depends on the synthesis, and it is usually found in the 10−20% range). At 175 K, the compound has completely reached the low-spin form with $\chi_M T \approx 0.24$ cm^3 mol^{-1} K. The two steps are separated by a rather less marked intermediate plateau and are estimated to be around 223 and 265 K.

Thermodynamic Parameters. Figure 5 shows a typical example of the calorimetric results on the heating mode (10 K min^{-1}) for compounds **2** and **4**. Thermograms at heating and cooling rates of 2, 5, and 10 K min^{-1} were made for both compounds. The transition temperatures were estimated by extrapolation at zero rate to discard the thermal lag produced by the finite heat conductance of the holder and sample.

An anomaly is observed in the heat-capacity curve of **2**.

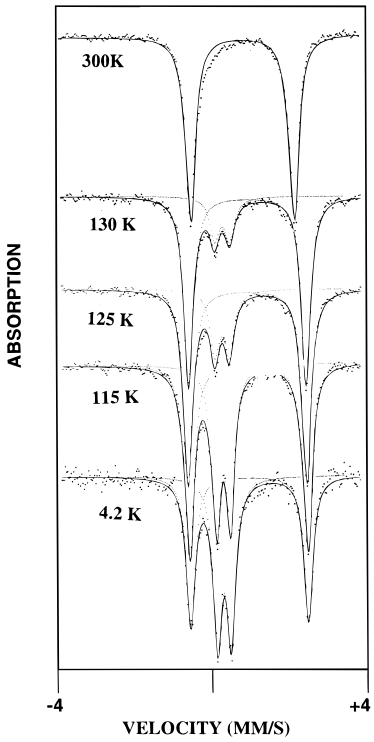

Figure 6. Selected Mössbauer spectra of **2**, obtained in the heating mode.

Slightly sharper curves are observed at lower heating rates. When the sample is cooled, the peak broadens and flattens to roughly one-half of its value on heating. The anomaly corresponds to a first-order transition showing a thermal hysteresis of 3.4 K, with a transition temperature $T_c(\uparrow) \approx 123.0 \pm 0.2$ K on heating. The anomalous enthalpy and entropy (referred to moles of formula units) have been estimated by intregration of the peaks giving $\Delta H = 3.0 \pm 0.1$ kJ mol^{-1} and $\Delta S = 25 \pm 1$ J mol^{-1} K^{-1}.

Compound **4** shows two different anomalies with maxima at $T_c(1) = 225.1 \pm 0.2$ K and $T_c(2) = 262 \pm 2$ K. The first peak is sharp like the one found for **2** but broader and with no hysteresis. The enthalpy and entropy (referred to moles of formula units) that were obtained for the peak was $\Delta H(1) = 5.7 \pm 0.3$ kJ mol^{-1}, $\Delta S(1) = 25.5 \pm 1$ J mol^{-1} K^{-1}. The anomaly that is centered at 262 K extends over a wide temperature range precluding a confident estimation of the enthalpy content. A rough estimate of ΔH and ΔS of the global spin conversion gave 16 kJ mol^{-1} and 65 J mol^{-1} K $^{-1}$, respectively.

It should be noted that the ΔS values that are obtained for **2** (second step) and **4** (first step) (≈ 25 J mol^{-1} K^{-1}) are smaller than most of literature data on mononuclear species ($\approx 30-80$ J mol^{-1} K^{-1}). However, their value is larger than the entropy variation due to a change of spin state alone, $\Delta S_{el} = R \ln[(2S+1)_{HS}/(2S+1)_{LS}] = 13.4$ J mol^{-1} K^{-1}. The excess value, *ca.* 12 J mol^{-1} K^{-1}, corresponds to the intramolecular vibration changes associated with the M−L stretching modes and the L−M−L deformation changes, including as well a certain contribution by lattice vibrations which usually is considered as minor.

Mössbauer Spectrometry Data. The temperature dependence of the ^{57}Fe Mössbauer spectra has been studied, for both **2** and **4**, between room temperature and 4.2 K. Figures 6 and 7 show a selection of some representative spectra that were obtained at increasing temperatures for **2** and **4**, respectively. The main doublet that is observed at 300 (**2**) and 304 K (**4**) is

Table 4. Least-Squares-Fitted Mössbauer Data[a] for Compounds **2** and **4**

	low-spin state			high-spin state			
T (K)	IS (mm s^{-1})	ΔE_q^{LS} (mm s^{-1})	$\Gamma/2$ (mm s^{-1})	IS (mm s^{-1})	ΔE_q^{HS} (mm s^{-1})	$\Gamma/2$ (mm s^{-1})	A_{HS}/A_{tot} (%)
			Compound **2**				
4.2	0.452(2)	0.357(3)	0.138 (3)	1.105(2)	3.073(4)	0.141(4)	49
45	0.452(3)	0.361(4)	0.139 (4)	1.118(2)	3.097(5)	0.156(4)	54
78	0.445(1)	0.360(2)	0.131 (1)	1.104(1)	3.088(2)	0.148(1)	54
115	0.438(2)	0.363(3)	0.138 (2)	1.092(1)	3.062(2)	0.150(2)	57
125	0.436(1)	0.377(5)	0.15	1.085(1)	3.062(2)	0.151(1)	76
130	0.431(5)	0.391(8)	0.15	1.083(1)	3.052(2)	0.148(1)	82
140	0.278(8)	0.39(1)	0.15	1.074(1)	3.031(2)	0.149(2)	87
178				1.056(3)	2.973(5)	0.153(4)	90
300				0.983(2)	2.685(3)	0.160(3)	92
			Compound **4**				
80	0.417(2)	0.406(3)	0.124(2)				0
180	0.395(1)	0.399(2)	0.127(2)	1.19(3)	2.68(5)	0.12(4)	4
210	0.385(2)	0.399(3)	0.127(3)	0.99(1)	2.64(3)	0.11(2)	9
220	0.382(2)	0.407(3)	0.128(3)	1.002(8)	2.58(2)	0.14(1)	20
230	0.369(3)	0.428(6)	0.140(4)	1.020(7)	2.58(2)	0.15(2)	31
240	0.370(5)	0.438(8)	0.136(6)	1.016(7)	2.490(1)	0.16(1)	44
260	0.340(7)	0.470(1)	0.178(8)	0.995(5)	2.411(9)	0.166(7)	54
280	0.280(2)	0.410(3)	0.260(3)	0.991(4)	2.365(8)	0.165(6)	64
304	0.276	0.410	0.480(1)	0.988(3)	2.259(6)	0.180(5)	75

[a] IS = isomer shift, ΔE_q = quadrupole splitting, Γ = half-height with of lines, A_{HS}/A_{tot} = area ratio. Statistical standard deviations given in brackets; italic values were fixed to the fit. Isomer shift values refer to metallic iron at 300 K. A = baseline-corrected area.

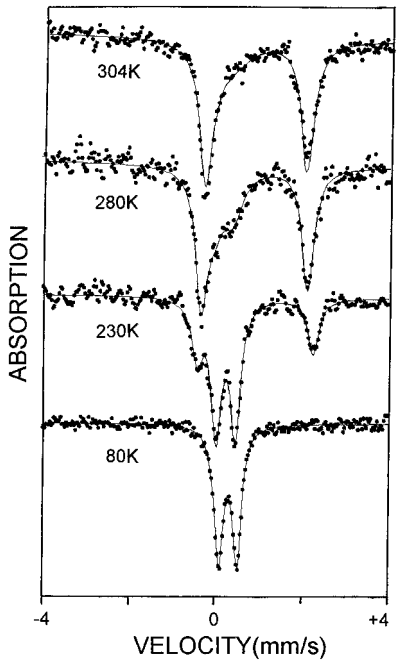

Figure 7. Selected Mössbauer spectra of **4**, obtained in the heating mode.

characterized by quadrupole splitting values of $\Delta E_q = 2.685$ (**2**) and 2.365 mm s^{-1} (**4**) and isomer shift values of IS = 0.983 (**2**) and 0.991 mms^{-1} (**4**). These values correspond to the $S = 2$ high-spin ground state of iron(II). As the temperature is lowered, another doublet appears (between the two previous peaks), the intensity of which increases at the expense of that of the first one. The fitted parameters at 4.2 K are $\Delta E_q = 0.357$ mm s^{-1} and IS = 0.452 mm s^{-1} for **2** and at 80K are $\Delta E_q = 0.406$ mm s^{-1} and IS = 0.417 mm s^{-1} for **4**. They are typical of the $S = 0$ low-spin state of iron(II). It should be noted that the fitting of the 304 K spectrum of **4** shows the presence of a significant residual low-spin fraction (up to *ca.* 25%) depending on the moisture content of the sample and is, therefore, partly due to nonintrisic effects. In contrast to **4**, **2** shows an additional doublet at 4.2 K that corresponds to *ca.* 50% of iron(II) in the high-spin form; such a value is too large for being due to a nonintrinsic effect and, rather, suggests that the plateau that is associated with the LS−HS state extends down to the lowest temperatures. In general, no spectrum deformation or line broadening is observable in this temperature range, indicating that the spin-conversion rates are slow compared to the hyperfine frequencies (*ca.* 10^8 s^{-1}). Only **4** shows broadening of the lines above 280 K, indicating that the spin-conversion frequency reaches a value close to that of the hyperfine frequency.[23]

Detailed values of the Mössbauer parameters resulting from least-squares fitting procedures are listed in Table 4 for a representative set of temperatures. The thermal variations of the area ratio $n_{HS} \approx A_{HS}/A_{tot}$ (A_{tot} and A_{HS} are the total and the high-spin area, respectively, of the Mössbauer spectra and n_{HS} the high-spin molar fraction) compare well with those deduced from the magnetic susceptibility measurements as shown in Figure 8 for compound **4**.

Discussion. The first goal dealt with the structural characterization of the spin crossover compounds **2**, **3**, and **4**. The EXAFS data for these compounds entirely match the structural features of **1**, which has been utilized as a model because its X-ray single-crystal structure is known. The EXAFS data show that the average Fe−N bond distance is close to 0.2 Å larger for the HS state than for the the LS state. Consequently, the LS → HS conversion is accompanied by a distortion of the [FeN_6] octahedron. The results also suggest that the Fe−N bond distance modification upon spin conversion is slightly greater for bt as the peripheral ligand than that for bpym as the bridging ligand in compounds **3** and **4**. This is in contrast to **2** which shows a slightly greater Fe−N bond distance modification for bpym as the bridging ligand than that for bpym as the peripheral one. All of the EXAFS-derived structural features agree with those of related mononuclear spin-crossover compounds.

The second point dealt with the interactions that are responsible for the two-step behavior. Following our previous interpretations of compound **3**, based on subtle variations of the Mössbauer parameters,[11] we assigned each dimeric molecule the following microscopic steps:

(23) (a) Adler, P.; Hauser, A.; Vef, A.; Spiering, H.; Gütlich, P. *Hyperfine Interact.* **1989**, *47*, 343. (b) Adler, P.; Spiering, H.; Gütlich, P. *J. Chem. Phys.* **1989**, *50*, 587.

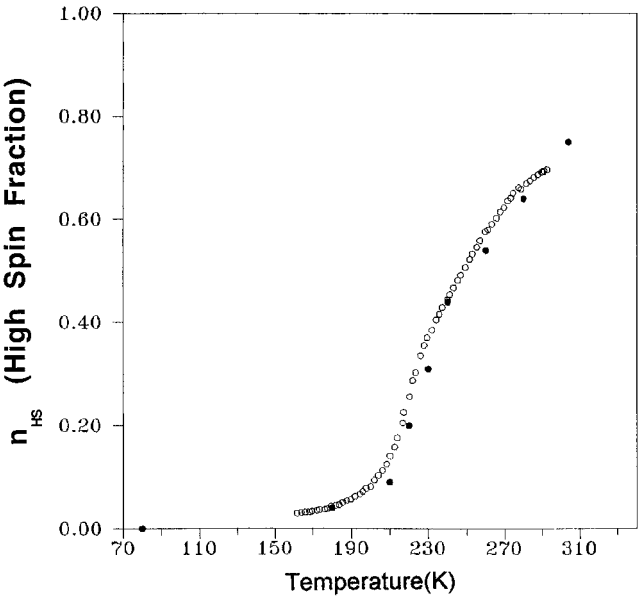

Figure 8. Thermal variation of the high spin fraction of **4** (n_{HS}); open and black circles correspond to magnetic susceptibility and to Mössbauer spectrometry data, respectively.

$$\text{LS}-\text{LS} \overset{1}{\leftrightarrow} \text{LS}-\text{HS} \overset{2}{\leftrightarrow} \text{HS}-\text{HS}$$

Cooperativity in a spin-crossover system requires the onset of intermolecular couplings, supposed to be "ferromagnetic-like", i.e., favoring homogeneous phases with dominating LS or HS character. The inhomogeneous LS−HS state which appears in the plateau temperature range can be stabilized through "antiferromagnetic-like" intramolecular couplings. Since couplings of both types are needed, the effect was termed "synergistic" (see ref 11).

The half transition exhibited by compound **2** has a clear meaning in the above microscopic description: the low-temperature state of the system is the mixed LS−HS state. In the frame of the binuclear Ising-like model,[12b] this only requires the following condition between parameter values to be fulfilled:

$$-J_{AB} > 2J + |\Delta|/2 \qquad (1)$$

where J_{AB} and J are the antiferromagnetic-like intramolecular and ferromagnetic-like intermolecular coupling parameters (expressed in terms of fictitious spins,[12a] with the sign convention of positive = ferromagnetic-like), respectively, and $\Delta = E_{HS} - E_{LS}$ is the energy gap of the isolated spin-crossover atoms.

It is worth noting that condition 1 is but an equilibrium condition and can be trespassed by metastable states that are associated with the hysteresis loop of the first-order transition; also, the slow kinetics of the spin conversion at low temperatures may prevent a first step existing in the conversion equilibrium curve below *ca.* 60 K from being observed. On the other hand, from a practical point of view, the half-conversion curve $n_{HS}(T)$ of compound **2** does not contain sufficient information for determining all of the parameters of the model.

For a quantitative modeling of the $n_{HS}(T)$ conversion curves, some of the parameters of the Ising-like model can be deduced from thermodynamic data, according to the following relations:

$$\Delta = \Delta H_{tot}/2N \qquad (2)$$

$$\log(g_{HS}/g_{LS}) = \Delta S_{tot}/2R \qquad (3)$$

$$\Delta H_{tot} = T_{1/2}\Delta S_{tot} \qquad (4)$$

where ΔH_{tot} and ΔS_{tot} are the enthalpy and entropy variations upon total conversion of a mole of binuclear complex (easily deduced from the calorimetric data), N is Avogadro's number, g_{HS} and g_{LS} are "effective" degeneracies accounting for both electronic degeneracies and densities of vibrational states,[24] and $T_{1/2}$ is the (equilibrium) half transition temperature, in the plateau; eq 4 has been straightforwardly derived from eq 5 of ref 12a.

As suggested by the experimental data of **3**, the model unambiguously shows that ΔS_{tot} is almost equally shared between the two steps of the transition: $\Delta S(1) \approx \Delta S(2) \approx \Delta S_{tot}/2$; of course, this is not true for ΔH. Consequently, the calorimetric data are treated as follows.

compound **2**:

$$\Delta S_{tot} \approx 2\Delta S(2) \approx 50 \text{ J K}^{-1} \text{ mol}^{-1} \ (g = g_{HS}/g_{LS} \approx 20)$$

compound **3**:

$$\Delta S_{tot} \approx 82 \text{ J K}^{-1} \text{ mol}^{-1} \text{ (ref 11)} \ (g = g_{HS}/g_{LS} \approx 138)$$

compound **4**:

$$\Delta S_{tot} \approx 2\Delta S(1) \approx 51 \text{ J K}^{-1} \text{ mol}^{-1} \ (g = g_{HS}/g_{LS} \approx 21)$$

These values clearly reveal the prominent role of the S/Se substitution in the entropy change value, such an effect is explained considering the major contribution of low-frequency intramolecular vibrations to ΔS,[11,25] the latter are obviously very sensitive to the presence of a heavy atom such as Se. On the other hand, ΔH values, originating from the ligand field, should be rather insensitive to the S/Se substitution occurring at the external tip of the NCX anionic ligand. Indeed, the experimental data for compounds **3** and **4** are rather close 14 and 16 kJ K^{-1} mol^{-1}, respectively. In contrast, as shown by comparing the equilibrium temperatures, $T_{1/2}$, of **1** and **2** to those of **3** and **4**, it is clear that ΔH depends strongly on the nature of the peripheral ligand, bpym or bt.

Then, the increase in the value of $T_{1/2}$ from **3** to **4** can be attributed mainly to the decrease in ΔS due to the vibrational effect of the S/Se substitution. The smoother character of the conversion curve of **4** does not involve a decrease in the coupling parameters, since the steepness of the conversion curve (as well as the onset of discontinuities) is governed by the reduced values of these parameters: $J/T_{1/2}$, $J_{AB}/T_{1/2}$.[12] Fitted parameter values are listed in Table 5, while corresponding computed conversion curves are shown in Figure 9. For the half transition of **2**, we have chosen parameter values as close as possible to fulfill eq 1, with a J_{AB} value that is close to the value already obtained for **2** and **3**. The needed change in J value can be explained by considering the sensitivity of (steric) intermolecular couplings to changes in the molecular unit geometry.[9] As already mentioned, several sets of parameters are possible, so that the values reported in Table 5 for **2** should not be considered as definitive.

From a general point of view, half transitions are fascinating and, so far, have been studied relatively little. Recently,[26] the LS−LS missing state has been reached by use of the reverse LIESST (light-induced excited spin state trapping) technique.

(24) Bousseksou, A.; Constant-Machado, H.; Varret, F. *J. Phys. I* **1995**, *5*, 747.
(25) Bousseksou, A. Ph. D. Thesis. Université Paris 6, 1992.
(26) (a) Hinek, R.; Hauser, A.; Gütlich, P. 2nd Spin Crossover Family Meeting (Gif sur Yvette 1995; private communication). (b) Hauser, A.; Jeftic, J.; Romstedt, H.; Hinek, R. *Mol. Cryst., Liquid Cryst.* in press.

Table 5. Parameters of the Ising-like Binuclear Model, Treated in Mean-Field Approximation

compound	Δ (K)	J (K)	$J_{AB\ (K)}$	g_{HS}/g_{LS}
2	270	130	−144	*20*
3	778	142	−122	*138*
4	749	160	*−122*	*20*

[a] Symbols have been defined in the text. Italic values have been fixed, according to the discussion. For **2**, only one among all possible solutions is given.

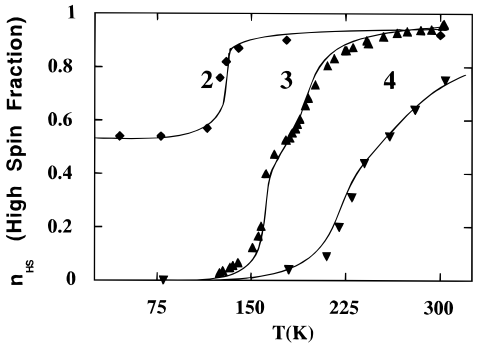

Figure 9. Computed conversion curves using the Ising-like model in mean-field approach (ref 12), fitted to the experimental Mössbauer data; parameter values are listed in Table 5.

In addition, applied pressure experiments might reveal the underlying two-step character of such systems. An open problem is that of the possible ordering of the LS−HS pairs in the lattice. For this problem, a full analogy with antiferromagnets might be usefully developed.

For **1**, which remains predominantly in the HS−HS state at most of temperatures, it is clear that the energy gap parameter Δ must be negative or, if positive, quite small.

The synthesis of new dinuclear spin-crossover compounds aimed at analyzing the intra- and intermolecular interactions that are responsible for this cooperative mechanism is one of our main goals in the near future. We will also focus our attention on the spin-conversion dynamic, with particular interest on the influence that the LS−HS state could induce on the well-established description of the molecular spin-crossover phenomenon as a nonadiabatic process between two energy wells.[27]

Acknowledgment. This work was financially supported by the Dirección General de Investigación Científica y Técnica (DGICYT, Spain) through Project PB95-1002 and the Human Capital and Mobility Program (Network on Magnetic Molecular Materials from ECC) through grant ERBCHRXCT920080. We also thank Professor J. P. Tuchagues (Toulouse) for his help with the Mössbauer experiments. J. A. Real thanks Professor O. Kahn (Bordeaux) and Dr. J. Zarembowitch (Orsay) who stimulated his interest on this topic and finally Professor M. Julve for his helpful discussions.

Supporting Information Available: Figure S1 contains the experimental $k\chi(k)$ spectra at 300 K for compounds **1**−**4** and at 77 K for **2**−**4** (1 page). Ordering information is given on any current masthead page.

IC960509O

(27) Buhks, E.; Navon, G.; Bixon, M; Jortner, J. *J. Am. Chem Soc*. **1980**, *102*, 2918.